The Bioscan
AN INTERNATIONAL QUARTERLY JOURNAL OF LIFE SCIENCES
20(4): 1352-1369, 2025 www.thebioscan.com

Formulation of Zolmitriptan Nanosponges Embedded in Fast-Dissolving Sublingual Films: A 3^2 Factorial Optimization Study

Adil Patel[1*], Rajesh Dodiya[2], Chirag Parmar[3], Nidhi Joshi[1]

[1]Ramanbhai Patel College of Pharmacy, Charotar University of Science and Technology (CHARUSAT), CHARUSAT Campus, Changa-388421, India.
E Mail: Adilpatel.ph@charusat.ac.in
[2]School of Pharmacy, Parul University, Vadodara, India
[3]Dept. of pharmaceutics, Shivam pharmaceutical studies and research centre, Valasan, India

DOI: 10.63001/tbs.2025.v20.i04.pp1352-1369

KEYWORDS
Zolmitriptan, Migraine, Nanosponge, Sublingual Film, Bioavailability, Emulsion Solvent Diffusion, Poly Vinayl Alcohol.

Received on:
07-10-2025

Accepted on:
13-11-2025

Published on:
24-12-2025

ABSTRACT

The Zolmitriptan is a serotonin (5- HT1) agonist used for the treatment of migraine with or without aura. The half-life of Zolmitriptan is 2.5 to 3 hr, the absolute oral bioavailability is about 40 to 50%. Hence the main objective of the study was to formulate & develop zolmitriptan loaded nanosponge based sublingual film to achieve a better permeability and further improving the bioavailability of the drug. Zolmitriptan nanosponge (ZMT-Ns) were prepared by emulsion solvent diffusion method and then encapsulated into the films by solvent casting method. 3^2 factorial design applied to analyses the influence of independent variables, concentration of polymer polyvinylalcohol, EC, on the responses for dependent variables, particle size, Entrapment Efficiency and PDI which were found to be 373nm, 93.23%,0.389. The drug release from nanosponges was found to extended up to 8h. Morphological characters were identified by scanning electron microscopy. Solid state characteristic of the drug in the formulation was evaluated by X-ray diffraction. FDSFs were evaluated for their disintegration time, weight variation, thickness, drug content, and surface ph. Stability studies were performed at 40 ± 2 °C/75 ± 5% RH. These results indicated that the ZMT-Ns FDSFs could be a promising delivery system to enhance the permeability and further improving the bioavailability of the drug.

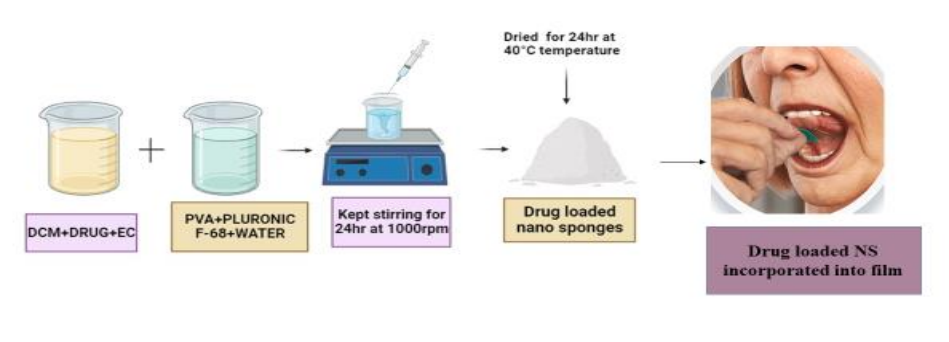

Introduction:

Migraine is a debilitating neurological disorder characterized by recurrent episodes of intense headache often accompanied by nausea, vomiting, and sensitivity to light or sound. Among the drugs used to treat migraines, Zolmitriptan, a serotonin (5-HT1) receptor agonist, is a well-established therapeutic agent. Zolmitriptan effectively alleviates migraine symptoms by promoting cranial vasoconstriction and inhibiting the release of neuropeptides involved in pain transmission. However, its oral bioavailability is limited to approximately 40-50% due to extensive hepatic first-pass metabolism and poor solubility, which hinder its therapeutic efficacy.[1-5]

To overcome these challenges, drug-loaded polymeric nanosponges have emerged as a

promising delivery system to enhance drug bioavailability. Nanosponges are tiny, porous structures capable of encapsulating hydrophilic or lipophilic drugs, providing controlled release and improved solubility. In the case of Zolmitriptan, incorporating it into nanosponge-based sublingual films offers a dual advantage: bypassing first-pass metabolism through the sublingual route and achieving sustained drug release. These nanosponges are typically prepared using emulsion solvent diffusion techniques and incorporated into sublingual films via solvent casting. By improving permeability and bioavailability, Zolmitriptan-loaded polymeric nanosponges have the potential to revolutionize migraine treatment, offering rapid relief and enhanced patient compliance while minimizing systemic side effects.[6-9]

Materials:

Zolmitriptan, Polyvinyl Alcohol and Pluronic F68 were procured from Yarrow Chem, Mumbai. Dichloromethane, Ethyl Cellulose, Hydroxypropyl Methylcellulose (HPMC E15), and Propylene Glycol were obtained from Loba Chemicals, Mumbai.

Methodology:

Preformulation studies:

FTIR spectra of the drug and ZMT-Ns were obtained using a Nicolet 6700 FTIR (Thermo Scientific, USA). Samples were ground and mixed with KBr to create an infrared-transparent matrix. Sample disks were prepared by compressing the mixtures with a pestle, and the spectrum was scanned at a resolution of 0.15 cm^{-1} with a scan speed of 20 scans/sec over a wavelength range of 4000–400 cm^{-1}.[10-12]

A DSC study was conducted to characterize ZMT, ZMT-Ns, and the physical state, encapsulation, and thermal modifications of ZMT in ZMT-Ns. DSC analysis was performed using a differential scanning calorimeter (DSC-60, Shimadzu Corporation, Japan) under nitrogen gas flow at a rate of 50 ml/min across a temperature range of 25–350°C with a heating rate of 10°C/min. Powder X-ray diffraction (D2-phaser, Bruker) was employed to determine the crystalline or amorphous state, encapsulation, and polymorphic changes in the drug during formulation. Patterns were recorded using Ni-filtered Cu Kα radiation at 40 kV and 20 mA, with a step size of 0.02° for 2s and a scanning speed of 10°/s in the 2θ range of 5–45°.[13-16]

Preparation of drug loaded Nanosponge:

Based on preliminary trials two factors were identified for further study. The experimental design consisted of nine batches, incorporating two factors and three levels. The effects of the independent variables on each of the three responses were evaluated using a 3^2 full factorial design for the optimized zolmitriptan-loaded nanosponges, as shown in the table. Optimization was performed using Design-Expert® software, version 13 by Stat-Ease, Inc. Various models were analyzed through one-way analysis of variance (ANOVA), 2D contour plots, and 3D surface plots. All possible interactions were examined to achieve maximum desirability and define the optimum design space.

The nanosponge was prepared using the emulsion solvent diffusion method. The aqueous phase was created by dissolving a measured quantity of PVA and PF-68 in distilled water. The drug and ethyl cellulose were dissolved in 30 mL of an organic phase containing dichloromethane. The organic phase was gradually added to the aqueous phase while maintaining continuous stirring at a speed of 1000–1200 revolutions per minute for 24 hours at ambient temperature. The resulting solution was filtered and then dried at 40°C.[17-23]

Characterization of drug loaded Nanosponge:

Particle size and Polydispersity Index (PDI):

The particle size and PDI of the optimized zolmitriptan nanosponges were measured using a Malvern Zetasizer 2000ms device (Malvern Instruments, Worcestershire, UK) and laser diffraction with a beam length of 2.40 mm and a refractive index (R.I) of 1.30.[25-27]

% Entrapment efficiency (%EE):

The entrapment efficiency (% EE) of drug-loaded nanosponges was calculated using an indirect method with a UV spectrophotometer. The prepared ZMT-Ns were dispersed and centrifuged at 10,000 rpm for 30 minutes using a cooling centrifuge to ensure the complete breakdown of the nanosponges. The unentrapped drug was separated from the supernatant and diluted with 0.1N HCl. The % EE was then calculated using the following formula, and the absorbance was measured with a UV spectrophotometer.[28-31]

$$\% \text{ EE} = \frac{\text{total amount of drug taken} - \text{unentrapped drug}}{\text{total amount of drug taken}} \times 100$$

Zeta-potential:

Zeta potential is measured by observing the movement of nanoparticles in an electric field, providing insight into their surface charge. Determining the zeta potential helps evaluate the surface charge of nanoparticles, which influences their stability and potential particle size growth. The zeta potential of the optimized ZMT-Ns was measured using a Malvern Zetasizer 2000MS device to assess their physical stability.[31-33]

***In vitro* drug release study of drug loaded nanosponge**

In-vitro drug release of ZMT-loaded nanosponge formulation was studied by dialysis method. The amount of drug released was measured using UV-spectrophotometer and the graph of % cumulative drug release vs time (min) was plotted, it was found that nanosponge formulation showed slower drug release for around 8 hr.[34,35]

Results:

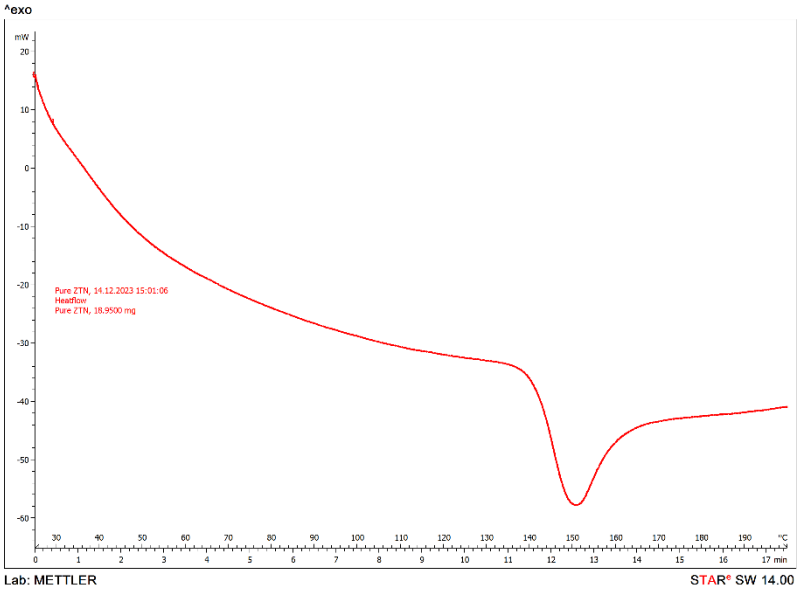

Figure 1: DSC thermograms of ZMT (Drug)

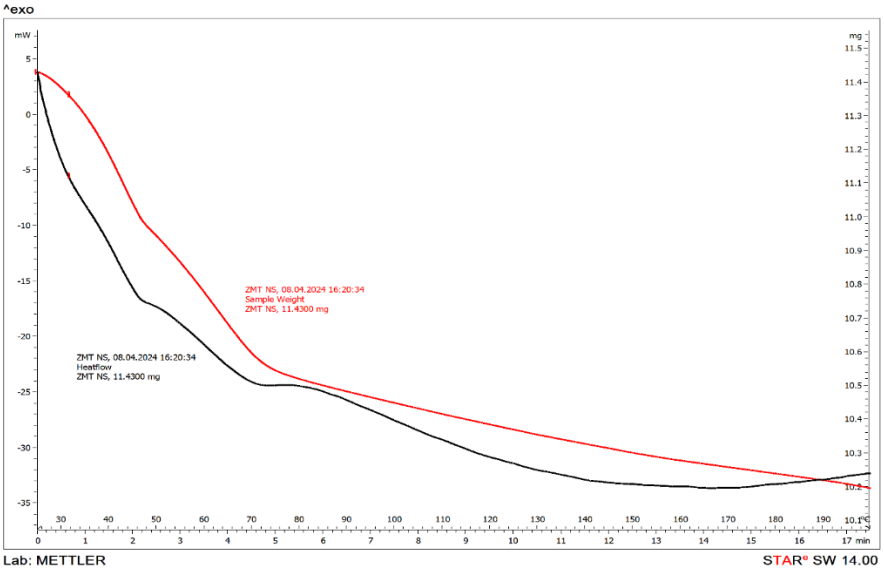

Figure 2: DSC thermograms of ZMT-Ns

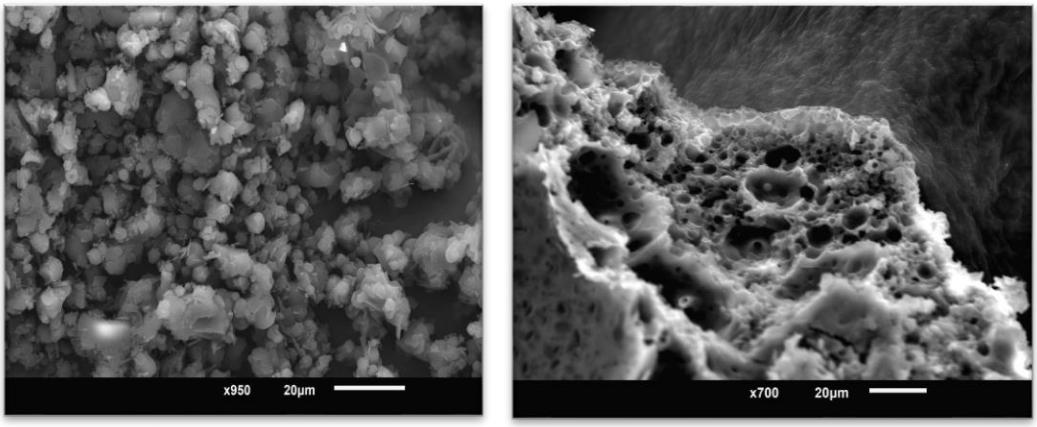

Figure 3: SEM analysis revealed Nano sized spherical particles with numerous pores on the surface

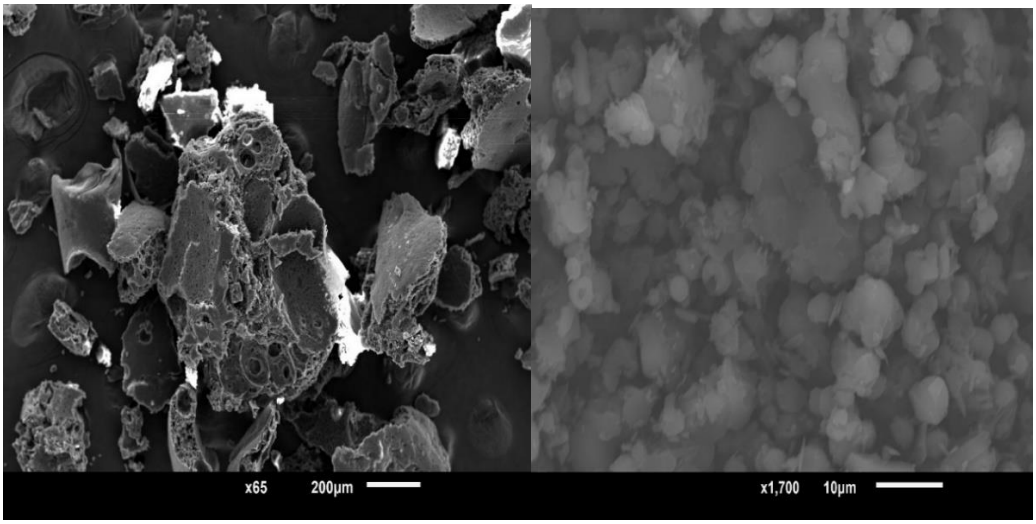

Figure 4: SEM image of ZMT-Ns

Results

		Size (d.nm...	% Intensity:	St Dev (d.n...
Z-Average (d.nm): 373	Peak 1:	395.5	96.8	91.67
PdI: 0.389	Peak 2:	5440	3.2	276.2
Intercept: 0.965	Peak 3:	0.000	0.0	0.000
Result quality Good				

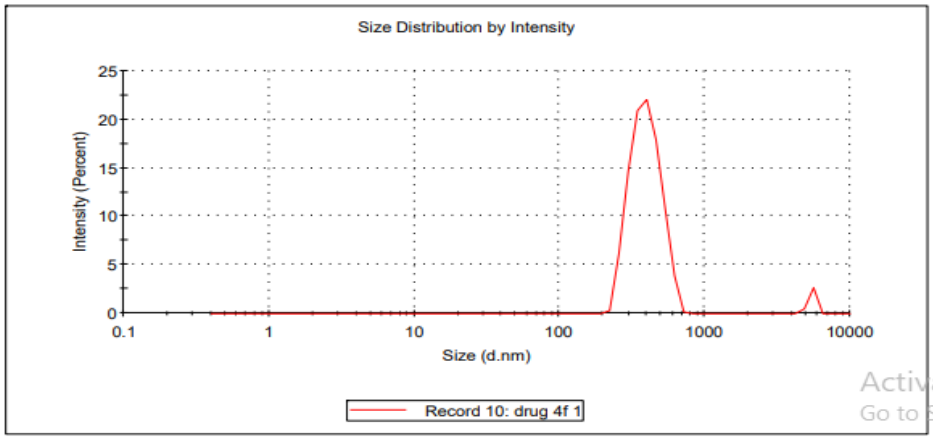

Figure 5: Particle size analysis report of optimized batch

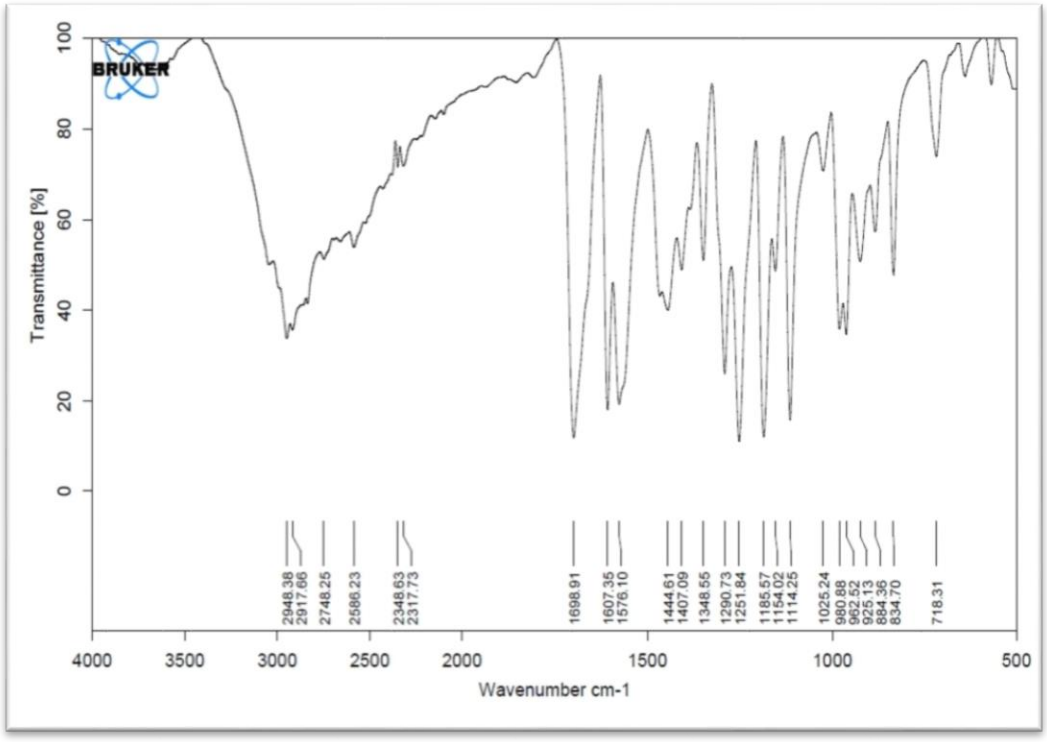

Figure 6: FTIR spectra of a physical mixture (Drug + EC + PVA+ Pluronic F-68)

Table 1: Results of Particle size analysis, PDI and % EE

	Factor 1	**Factor 2**	**Response 1**	**Response 2**	**Response3**
Batch code	**EC**	**PVA**	**Particle size**	**PDI**	**% Entrapment efficiency**
B1	400mg	600mg	555nm	0.302	65.47%
B2	400mg	900mg	433nm	0.316	70.55%
B3	400mg	1200mg	398nm	0.325	73.21%
B4	700mg	600mg	483nm	0.337	85.50%
B5	700mg	900mg	445nm	0.350	86.60%
B6	700mg	1200mg	373nm	0.389	92.23%
B7	1000mg	600mg	603nm	0.424	80.22%
B8	1000mg	900mg	586nm	0.480	81.59%
B9	1000mg	1200mg	571nm	0.551	83.43%

Table 2: Results of the different models for particle size

Model	**Standard deviation**	**R^2**	**Adjusted R^2**	**Predicted R^2**	**Significance/ non significance**
Linear	60.39	0.6593	0.5145	0.1123	
2FI	59.96	0.7009	0.5214	-0.4098	
Quadratic	**21.35**	**0.9773**	**0.9393**	**0.7769**	**Suggested**
Cubic	26.17	0.9886	0.9089	-1.0765	**Aliased**

Table 3: ANOVA data for particle size (Quadratic model)

Source	Sum of Squares	DF	Mean Square	F-value	p-value
Model	58728.03	5	11745.61	25.78	0.0114
A-EC	23312.67	1	23312.67	51.17	0.0056
B-PVA	14900.17	1	14900.17	32.70	0.0106
AB	3906.25	1	3906.25	8.57	0.0611
A^2	16440.89	1	16440.89	36.08	0.0092
B^2	168.06	1	168.06	0.3688	0.5865
Residual	1366.86	3	455.62		
Cor Total	60094.89	8			

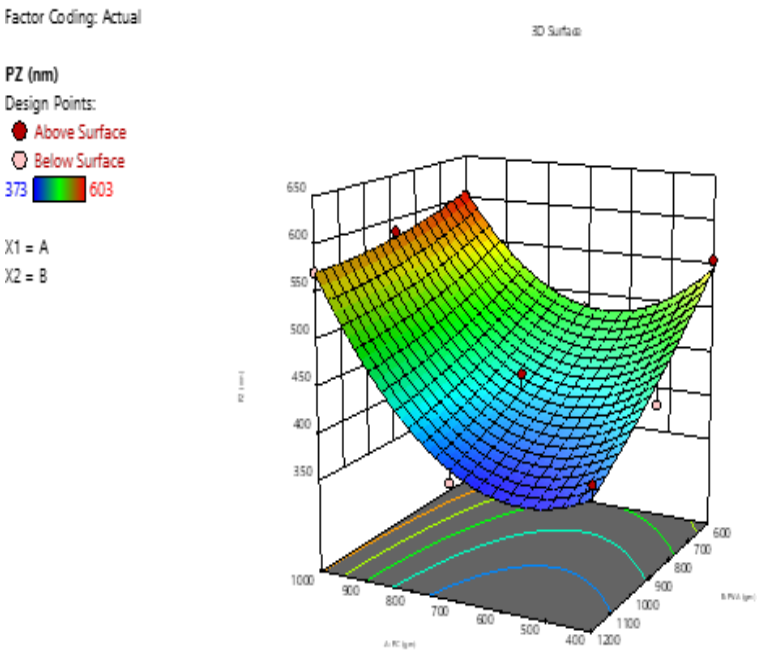

Figure 7: 3D Surface plot of particle size

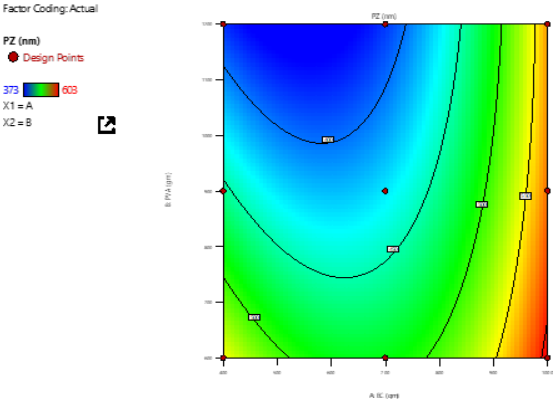

Figure 8: 2D Contour plot of particle size

Table 4: Results of the different models for PDI

Model	**Standard deviation**	**R^2**	**Adjusted R^2**	**Predicted R^2**	**Significance/ non significance**
Linear	0.0324	0.8885	0.8514	0.7182	
2FI	0.0270	0.9354	0.8967	0.7524	
Quadratic	**0.0091**	**0.9956**	**0.9882**	**0.9504**	**Suggested**
Cubic	0.0072	0.9991	0.9927	0.8345	Aliased

Table 5: ANOVA data for PDI (Quadratic model)

Source	**Sum Of Squares**	**DF**	**Mean Square**	**F-value**	**P-value**
Model	0.0563	5	0.0113	135.04	0.0010
A-EC	0.0435	1	0.0435	521.84	0.0002
B-PVA	0.0067	1	0.0067	80.74	0.0029
AB	0.0027	1	0.0027	31.80	0.0110
A^2	0.0033	1	0.0033	39.99	0.0080
B^2	0.0001	1	0.0001	0.8160	0.4329
Residual	0.0003	3	0.0001		
Cor Total	0.0566	8			

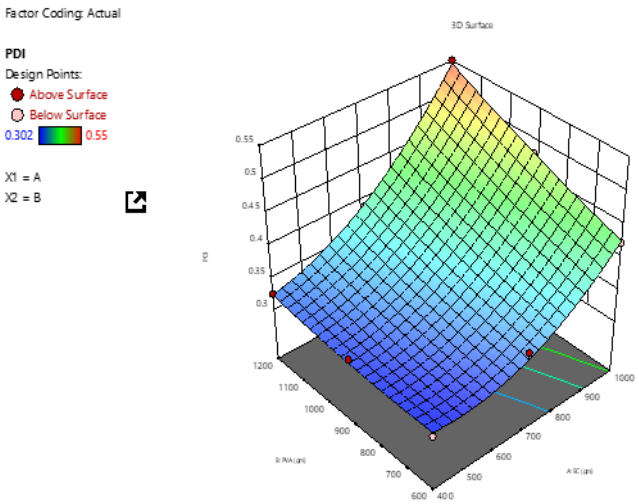

Figure 9: 3D Surface plot of PDI

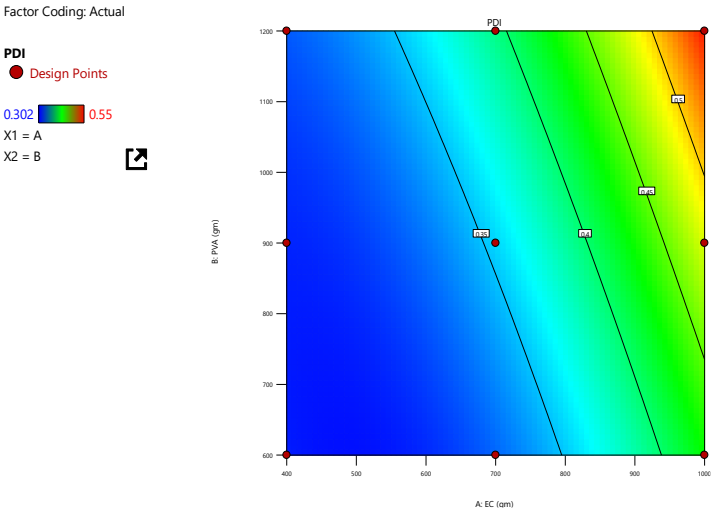

Figure 10: 2D Contour plot of PDI

Table 6: Results of the different models for % EE

Model	**Standard deviation**	**R^2**	**Adjusted R^2**	**Predicted R^2**	**Significance/ non significance**
Linear	7.39	0.4356	0.2475	-0.1989	
2FI	8.03	0.4444	0.1111	-1.0651	
Quadratic	**1.29**	**0.9915**	**0.9772**	**0.9119**	**Suggested**
Cubic	1.40	0.9966	0.9731	0.3876	Aliased

Table 7: ANOVA data for %EE (Quadratic model)

Source	**Sum of Squares**	**DF**	**Mean Square**	**F-value**	**p-value**
Model	575.55	5	115.11	69.66	0.0027
A-EC	201.03	1	201.03	121.65	0.0016
B-PVA	51.86	1	51.86	31.38	0.0112
AB	5.11	1	5.11	3.09	0.1770
A^2	316.09	1	316.09	191.28	0.0008
B^2	1.46	1	1.46	0.8813	0.4171
Residual	4.96	3	1.65		
Cor Total	580.51	8			

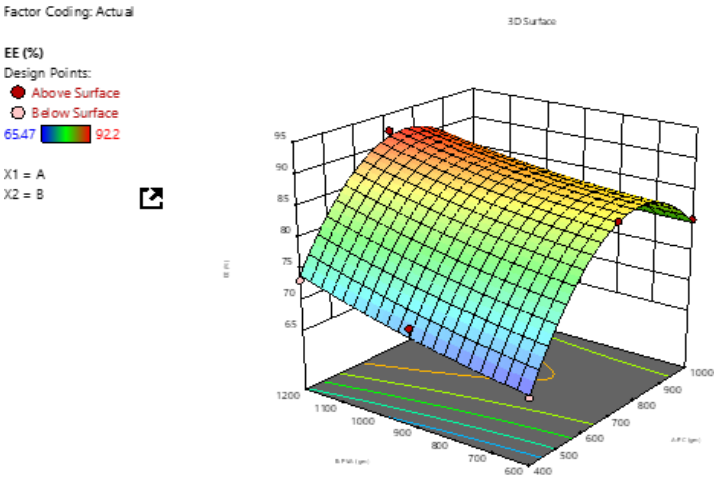

Figure 11: 3D Surface plot of %EE

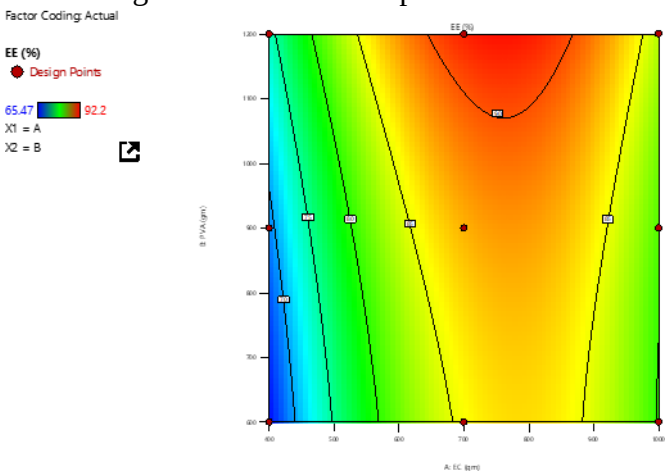

Figure 12: 2D Contour plot of %EE

Table 8: Optimized batch selected from the solutions

A: Amount of EC (mg)	B: Amount of PVA (mg)	Particle size (nm)	PDI	%EE	Desirability
700	1200	381.72	0.394	91.32%	0.951

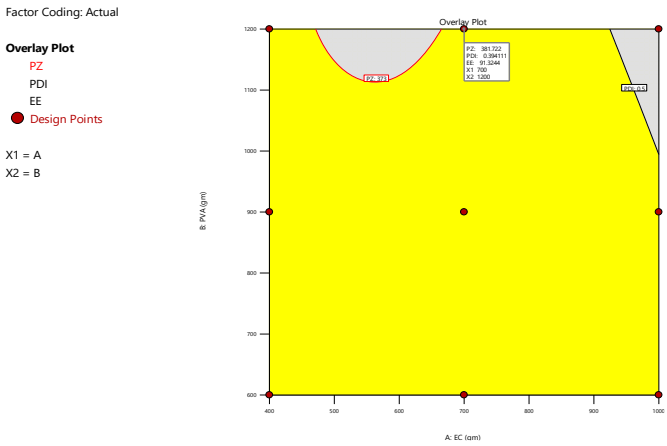

Figure 13: Overlay contour plot of prepared drug loaded Nano sponges (Design space)

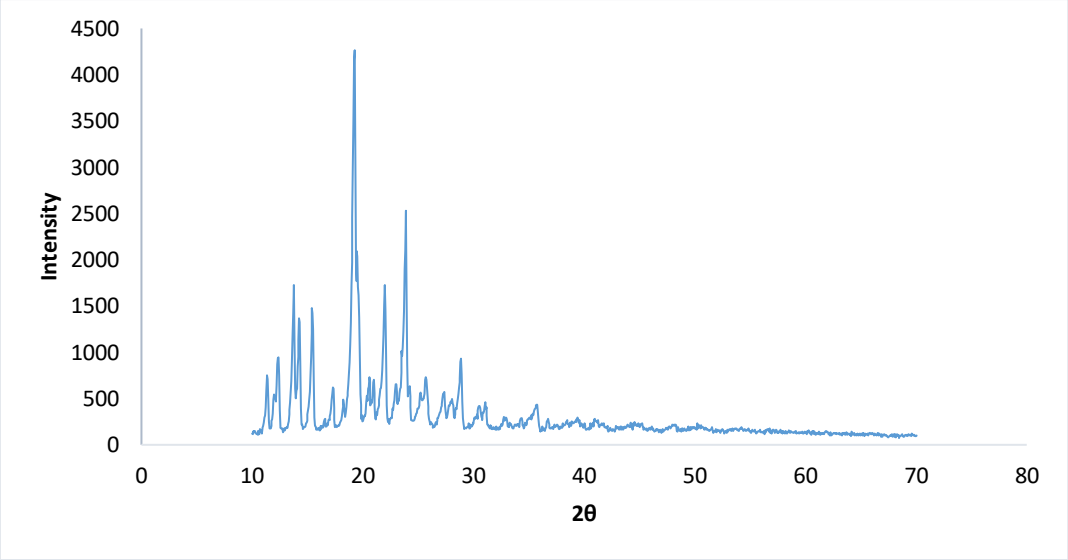

Figure 14: p-XRD spectra of ZMT

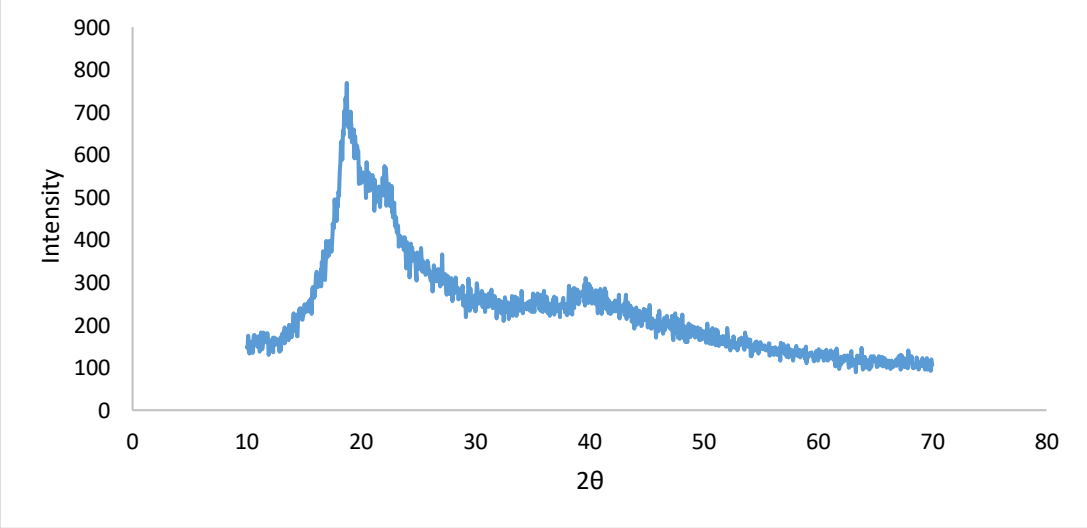

Figure 15: p-XRD spectra of ZMT-Ns

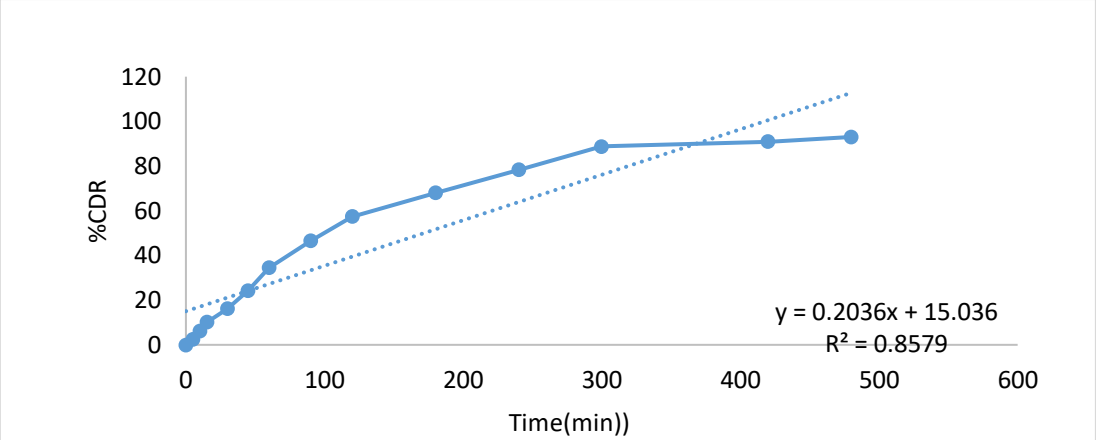

Figure 16: *In vitro* drug release of ZMT-Ns (B6**)**

Table 9: Regression co-efficient (R^2) values of different

MODELS	ZERO ORDER	FIRST ORDER	HIGUCHI	KORSHMEYER PEPAS
R^2	0.8915	0.5828	**0.9815**	0.9573

Results and discussion:

Determination of melting point:

Melting point determination was carried out using two methods capillary fusion method and differential scanning calorimetry. The melting point obtained from both methods was found to be similar to the reported melting point of the pure zolmitriptan powder 136-141℃ shown in table. The sharp utilized peak obtained at the melting point of ZMT as shown in figure indicates that the purchased ZMT powder is in pure form.

Structural determination by fourier transform infrared spectroscopy:

The obtained FTIR spectrum of purchased zolmitriptan was recorded. Figure 6 shows the FTIR spectrum of zolmitriptan, which comprises all of the typical peaks of specific functional groups found in the structure of zolmitriptan. All of the observed peaks of different functional groups were compared to the standard frequency of functional groups, as shown in Table and it was found that there was no considerable difference between the observed and standard frequencies. This concluded that the purchased drug was pure, free of adulteration or impurities.

Particle size analysis, PDI and %EE:

This study investigated the influence of two main factors, EC and PVA concentrations, on the properties of a formulation, including particle size, polydispersity index (PDI), and % entrapment efficiency (% EE), across nine experimental batches (B1 to B9).

The results show a clear interaction between the factors and responses. Increasing the concentration of PVA consistently led to a decrease in particle size (e.g., from 555nm to 398nm at 400mg EC), likely because PVA acts as a stabilizer that prevents particle coalescence. Conversely, increasing the concentration of the wall material EC consistently resulted in an

increase in particle size (e.g., from 398nm to 571nm at 1200mg PVA).

The statistical analysis for optimizing Particle Size (PZ) definitively established the Quadratic Model as the best fit, validated by its high R^2 (0.9773), low Standard Deviation (21.35), and good predictive power (Predicted R^2 of 0.7769). The ANOVA results confirmed the model's overall significance ($p=0.0114$) and identified both EC (A) and PVA (B) concentrations as highly significant factors influencing particle size ($p<0.05$). Specifically, the linear effects of both factors were significant, as was the non-linear effect of EC (indicated by the significant A2 term, $p=0.0092$). The Response Surface and Contour plots visually interpret these findings: increasing the concentration of the wall material EC consistently increased the particle size, which is chemically logical due to the greater mass available for particle formation, while increasing the stabilizer PVA concentration consistently decreased the particle size by enhancing surface stabilization and preventing coalescence. This complex relationship indicates that the minimum particle size (ranging from 373nm to 400nm) is achieved in the region defined by low-to-intermediate EC concentrations combined with high PVA concentrations, representing the optimal balance between providing sufficient material for the particle core and maximizing stabilization.

Regarding efficiency, increasing both EC and PVA concentrations positively impacted the % Entrapment Efficiency. Higher EC provided a more substantial wall to trap the active material, while higher PVA likely stabilized the system more quickly. The % EE ranged from a low of 65.47% (B1) to a high of 92.23% (B6).

The optimization study for % Entrapment Efficiency (% EE), which ranged from a minimum of 65.47% to a maximum of 92.2%, established the Quadratic Model as the most suitable one. This selection is justified by its exceptionally high R^2 value (0.9915), low Standard Deviation (1.29), and robust predictive capability (Predicted R^2 of 0.9119). The ANOVA confirmed the model's high statistical significance ($p=0.0027$) and highlighted that both factors significantly influence % EE. The concentration of EC (A), the wall material, was the primary driver, showing the highest significance for both its linear ($p=0.0016$) and quadratic (A2, $p=0.0008$) terms. PVA (B) also exhibited a significant linear effect ($p=0.0112$), while the interaction term (AB) was not statistically significant ($p=0.1770$). The 3D surface and contour plots clearly illustrate that increasing the concentration of EC drastically increases the % EE, pushing the response from the low-efficiency blue region towards the high-efficiency red region. This is expected, as more polymer provides a thicker matrix to encapsulate the drug and prevent leakage. PVA also positively contributed to % EE (the surface slopes upwards along the PVA axis), likely by stabilizing the droplets and promoting a faster encapsulation process. The maximum % EE (the peak of the surface, ≈92.2%) is achieved by using intermediate-to-high concentrations of EC (≈700mg to 1000mg) and high concentrations of PVA (≈1000mg to 1200mg), demonstrating that optimizing both the wall material and the stabilizing phase is crucial for maximizing drug retention.

However, the Polydispersity Index (PDI), which measures particle uniformity, generally increased with higher concentrations of both EC and PVA, suggesting a less uniform particle population. The most uniform particles (lowest PDI, 0.302) were found in B1 (lowest EC and PVA), while the least uniform (highest PDI, 0.551) were in B9 (highest EC and PVA).

The statistical analysis for the Polydispersity Index (PDI) established the Quadratic Model as the optimal fit, evidenced by its exceptional R^2 of 0.9956 and its strong predictive capability. The ANOVA confirmed the model's overall highly significant influence on PDI (p=0.0010). Analysis of the individual factors revealed that the concentration of EC (A) was the most dominant factor, showing a highly significant linear (p=0.0002) and non-linear (A2, p=0.0080) effect on PDI. The concentration of PVA (B) was also highly significant (p=0.0029), and a significant interaction term (AB, p=0.0110) indicated that the effect of one polymer was dependent on the level of the other. The 3D surface and contour plots visually confirm that increasing the concentration of the polymer (EC) dramatically increases the PDI, pushing the values toward the less uniform red region (up to 0.55). This is attributed to the increased viscosity at higher polymer loads, which hinders efficient homogenization and leads to a wider range of particle sizes. Conversely, the optimal uniformity (minimum PDI of ≈0.302) is achieved in the deep blue region where both EC and PVA concentrations are at their lowest levels. This highlights the trade-off inherent in the formulation, where achieving optimal uniformity requires minimizing the polymer and stabilizer concentrations.

Overall, Batch B6 (700mg EC, 1200mg PVA) represented the most favourable compromise, achieving the highest % EE (92.23%) and a desirable small particle size (373nm), despite having a moderate PDI (0.389). This suggests that a medium polymer load (EC) coupled with a high stabilizer concentration (PVA) is optimal for maximizing both entrapment and particle minimization.

The powder X-ray Diffraction (p-XRD) analysis:

The powder X-ray Diffraction (p-XRD) analysis conclusively demonstrated a significant change in the solid-state nature of the material after nanonization. The spectrum of the raw ZMT material, figure 14, showed numerous sharp, high-intensity peaks (e.g., strong signals near 2θ values of 12°, 14°, 18°, 20°, and 25°), which is the classic signature of a highly crystalline structure. In sharp contrast, the spectrum of the ZMT-Ns nanoparticles, figure 15, displayed only a broad, diffuse halo or hump with a maximum intensity around 20°, and the original sharp characteristic peaks were absent. This transformation confirms that the nanonization process successfully converted the highly crystalline ZMT into an amorphous or near-amorphous form. This solid-state conversion is a highly desirable outcome for enhancing drug performance, as the disrupted, less-ordered amorphous state possesses significantly higher free energy, which is expected to lead to a substantial increase in the saturation solubility and dissolution rate of the ZMT drug, thereby potentially improving its overall bioavailability.

In Vitro Drug Release Study:

The analysis of the In Vitro Drug Release Study revealed that the release kinetics are best described by the Higuchi model, which yielded the highest coefficient of determination (R^2=0.9815). This excellent fit indicates that the drug release mechanism from the formulated nanoparticles is primarily governed by Fickian diffusion through the polymer matrix, which is assumed to be non-disintegrating or sparingly soluble. Although the Korshmeyer-Peppas model also provided a strong fit (R^2=0.9573), its correlation with the Higuchi model suggests that diffusion is the rate-limiting step. Conversely, the Zero-Order model offered only a moderate fit (R^2=0.8915), and the First-Order model was a poor descriptor (R^2=0.5828), confirming that the

release rate is not constant over time nor dependent on the concentration of drug remaining in the system. The observed release profile shows an initial rapid phase followed by a plateau after approximately 300min, a pattern consistent with a diffusion-controlled process where the rate slows as the diffusion path length increases over time.

Conclusion:

The overall findings confirm the successful development and characterization of zolmitriptan-loaded nanosponges with desirable physicochemical and performance attributes. Purity analysis through melting point determination and FTIR verified that the purchased ZMT was pure and free from impurities, while p-XRD confirmed its transformation from a highly crystalline to an amorphous form after nanonization, a change expected to enhance solubility and bioavailability. Optimization studies demonstrated that EC and PVA concentrations significantly influenced particle size, PDI, and entrapment efficiency, with the quadratic model providing the best predictive accuracy for all responses. Higher EC increased particle size and %EE but also led to broader particle distribution, whereas higher PVA effectively reduced particle size and improved stability. Batch B6 emerged as the optimal formulation, achieving a favourable balance of small particle size (373 nm), high entrapment efficiency (92.23%), and acceptable PDI. Finally, the in vitro drug release study confirmed Higuchi diffusion as the dominant release mechanism, indicating a sustained and diffusion-controlled release profile suitable for improved therapeutic performance.

References:

1. Ong JJY, Wei DYT, Goadsby PJ. Recent Advances in Pharmacotherapy for Migraine Prevention: From Pathophysiology to New Drugs. Drugs [Internet]. 2018;78(4):411–37. Available from: https://doi.org/10.1007/s40265-018-0865-y
2. Yeh WZ, Blizzard L, Taylor B V. What is the actual prevalence of migraine ? 2018;(January):6–11.
3. Aguilar-Shea AL, Diaz-de-Teran J. Migraine review for general practice. Aten Primaria [Internet]. 2022;54(2). Available from: https://doi.org/10.1016/j.aprim.2021.102208
4. Ashina M, Katsarava Z, Do TP, Buse DC, Pozo-Rosich P, Özge A, et al. Migraine: epidemiology and systems of care. Lancet. 2021;397(10283):1485–95.
5. Amiri P, Kazeminasab S, Nejadghaderi SA, Mohammadinasab R, Pourfathi H, Araj-Khodaei M, et al. Migraine: A Review on Its History, Global Epidemiology, Risk Factors, and Comorbidities. Front Neurol. 2022;12(February):1–15.
6. Lipton RB, Bigal ME. Migraine: Epidemiology, impact, and risk factors for progression. Headache. 2005;45(SUPPL. 1).
7. Goadsby PJ. Pathophysiolo gy of Migraine. Neurol Clin NA [Internet]. 2009;27(2):335–60. Available from: http://dx.doi.org/10.1016/j.ncl.2008.11.012
8. Goadsby PJ, Holland PR, Martins-Oliveira M, Hoffmann J, Schankin C, Akerman S. Pathophysiology of migraine: A disorder of sensory processing. Physiol Rev. 2017;97(2):553–622.
9. Villar-Martinez MD, Goadsby PJ. Pathophysiology and Therapy of Associated Features of Migraine. Cells. 2022;11(17):1–22.
10. Robbins MS, Burch R. Preventive Migraine Treatment. Contin Lifelong Learn Neurol.

2021;27(3):613–32.
11. DeMaagd G. The pharmacological management of migraine, part 2: Preventative therapy. P T. 2008;33(8):480–7.
12. Klapper J, Lucas C, Røsjø, Charlesworth B. Benefits of treating highly disabled migraine patients with zolmitriptan while pain is mild. Cephalalgia. 2004;24(11):918–24.
13. Palmer KJ, Spencer CM. Zolmitriptan. 1997;7(6):468–78.
14. Millson DS, Tepper SJ, Rapoport AM. Migraine pharmacotherapy with oral triptans: A rational approach to clinical management. Expert Opin Pharmacother. 2000;1(3):391–404.
15. Goswami T, Jasti BR, Li X. Sublingual drug delivery. Crit Rev Ther Drug Carrier Syst. 2008;25(5):449–84.
16. Hua S. Advances in nanoparticulate drug delivery approaches for sublingual and buccal administration. Front Pharmacol. 2019;10(November):1–9.
17. Mostafavi E, Iravani S, Varma RS. Nanosponges: An overlooked promising strategy to combat SARS-CoV-2. Drug Discov Today. 2022;27(10).
18. Panda S, Vijayalakshmi S, Pattnaik S, Swain RP. Nanosponges: A novel carrier for targeted drug delivery. Int J PharmTech Res. 2015;8(7):213–24.
19. Patel JK. REVIEW-SUBLINGUAL ROUTE FOR SYSTEMIC DRUG DELIVERY Volume ISSN : 2023;(May).
20. Tiwari K, Bhattacharya S. The ascension of nanosponges as a drug delivery carrier: preparation, characterization, and applications. J Mater Sci Mater Med. 2022;33(3).
21. Mali K, Patil N, Patil T, Raysing S, Surana S. Formulation and Evaluation of Transdermal Drug Delivery System Containing Anti-Inflammatory Agent. Int J Adv Res. 2018;6(2):1226–36.
22. Shrestha S, Bhattacharya S. Versatile Use of Nanosponge in the Pharmaceutical Arena: A Mini-Review. Recent Pat Nanotechnol. 2020;14(4):351–9.
23. Amin O, Ammar A, Eladawy SA. Ethylcellulose Based Nanosponges as Drug Carriers for Febuxostat. Int J Pharm Pharm Res. 2019;16(4):310–22.
24. Aher SS, Kayastha AR, Saudagar RB. Formulation Development and Evaluation of Sublingual Film of Nadolol. Eur J Biomed Pharm Sci [Internet]. 2017;4(8):524–32. Available from: www.ejbps.com
25. Jadhav N V., Vavia PR. Supercritical processed starch nanosponge as a carrier for enhancement of dissolution and pharmacological efficacy of fenofibrate. Int J Biol Macromol [Internet]. 2017;99:713–20. Available from: http://dx.doi.org/10.1016/j.ijbiomac.2017.03.002
26. Song Q, Shen C, Shen B, Lian W, Liu X, Dai B, et al. Development of a fast dissolving sublingual film containing meloxicam nanocrystals for enhanced dissolution and earlier absorption. J Drug Deliv Sci Technol [Internet]. 2018;43(September 2017):243–52. Available from: http://dx.doi.org/10.1016/j.jddst.2017.10.020
27. Penjuri SCB, Ravouru N, Damineni S, Bns S, Poreddy SR. Lasoprazol yüklü nanosüngerlerin formülasyonu ve değerlendirilmesi. Turkish J Pharm Sci. 2016;13(3):304–10.
28. El-Setouhy DA, Basalious EB, Abdelmalak NS. Bioenhanced sublingual tablet of drug with limited permeability using novel surfactant binder and

microencapsulated polysorbate: In vitro/in vivo evaluation. Eur J Pharm Biopharm [Internet]. 2015;94:386–92. Available from: http://dx.doi.org/10.1016/j.ejpb.2015.06.006

29. Time D, Tasdemir U, Erol H, Ozkan CK, Savaser A, Ozkan Y. Formulation of zolmitriptan sublingual tablets prepared by direct compression with different polymers: In vitro and in vivo evaluation. Eur J Pharm Biopharm [Internet]. 2011;78(3):499–505. Available from: http://dx.doi.org/10.1016/j.ejpb.2011.02.014
30. Ahmed MM, Fatima F, Anwer MK, Ibnouf EO, Kalam MA, Alshamsan A, et al. Formulation and in vitro evaluation of topical nanosponge-based gel containing butenafine for the treatment of fungal skin infection. Saudi Pharm J [Internet]. 2021;29(5):467–77. Available from: https://doi.org/10.1016/j.jsps.2021.04.010
31. Zainuddin R, Zaheer Z, Sangshetti JN, Momin M. Enhancement of oral bioavailability of anti-HIV drug rilpivirine HCl through nanosponge formulation*. Drug Dev Ind Pharm [Internet]. 2017;43(12):2076–84. Available from: https://doi.org/10.1080/03639045.2017.1371732
32. Acharjya SK, Rao MEB, Kumar BVVR, Annapurna MM. Journal of Advanced Scientific Research UV-Spectrophotometric Methods For The Determination Of Zolmitriptan in Bulk and Pharmaceutical Dosage Forms. J Adv Sci Res [Internet]. 2011;2(3):42–7. Available from: http://www.sciensage.info/jasr
33. Abd El-Halim SM, Mamdouh MA, Eid SM, Ibrahim BMM, Labib DAA, Soliman SM. The potential synergistic activity of zolmitriptan combined in new self-nanoemulsifying drug delivery systems: Atr-ftir real-time fast dissolution monitoring and pharmacodynamic assessment. Int J Nanomedicine. 2021;16(September):6395–412.
34. Choi DH, Kim YS, Kim DD, Jeong SH. QbD based development and evaluation of topical microemulsion-based hydrogel against superficial fungal infections. J Pharm Investig [Internet]. 2019;49(1):87–103. Available from: http://dx.doi.org/10.1007/s40005-018-0386-4
35. Bharti K, Mittal P, Mishra B. Formulation and characterization of fast dissolving oral films containing buspirone hydrochloride nanoparticles using design of experiment. J Drug Deliv Sci Technol [Internet]. 2019;49(December 2018):420–32. Available from: https://doi.org/10.1016/j.jddst.2018.12.013